Mesoporous Silica Nanoparticles with Manganese and Lanthanide Salts: Synthesis, Characterization and Cytotoxicity studies

Andreia Forte, Sandra Gago, Manuela Ribeiro Carrott, Peter Carrott, Celso Alves, Fernando Teodoro, Rui Pedrosa, Isabel M. Marrucho and Luis C. Branco

Dalton Trans., 2021, **50**, 8588-8599

DOI: 10.1039/d1dt00605c

ARTICLE

Mesoporous Silica Nanoparticles with Manganese and Lanthanide Salts: Synthesis, Characterization and Cytotoxicity studies

Received 00th January 20xx,
Accepted 00th January 20xx

DOI: 10.1039/x0xx00000x

Andreia Forte[a,b], Sandra Gago[a]*, Manuela Ribeiro Carrott[c], Peter Carrott[c], Celso Alves[d], Fernando Teodoro[d], Rui Pedrosa[d], Isabel M. Marrucho[b,e] and Luis C. Branco[a]*

Several organic salts based on the combination of two different choline derivative cations and $MnCl_3^-$, $GdCl_4^-$ and $TbCl_4^-$ as anions, were immobilized in mesoporous silica nanoparticles (MSNs) by a two-step synthetic method. Firstly, MSNs were functionalized with choline derivative cations with chloride anions and then the metals were incorporated by the reaction of the chloride with the respective metal chloride salts. These nanomaterials were fully characterized by different characterization techniques such as ^{1}H-NMR, FT-IR, elemental analysis, TEM, TGA, N_2 adsorption, XRD and DLS. These characterization data were important to confirm the successful functionalization of the nanomaterials and to access their textural properties and colloidal stability. The final materials were also characterized by ICP-MS that indicated the metal contents. The cytotoxicity profile was evaluated in four different cell lines (3T3, 293T, HepG2 and Caco-2), which shows some relevant differences between the metal organic salts and their immobilized analogues.

1. Introduction

Nanotechnology has attracted great attention in the last few years due to the possibility to produce a wide range of nanomaterials with different properties and compositions.[1] Among these nanomaterials, Mesoporous Silica Nanoparticles (MSNs) have been widely explored due to their properties such as high chemical stability, high specific surface area, tuneable particle and pore sizes, and narrow pore size distribution. The biocompatibility of MSNs and the possibility of functionalizing them with specific molecules either on the internal surface of their pores or on the external particle surface are their major advantages. [2–4]

Ionic Liquids (ILs) are a class of compounds that has attracted interest from academic and industrial communities in the last few years.[5]

They are usually defined as organic salts completely composed of ions with a melting point below 100 °C. One of the main features of these salts is the possibility of tuning their physical-chemical properties by applying different combinations of cations and anions scaffolds. This ability can create a large variety of IL structures for different applications. [6,7] Recently, a new class of these task-specific salts known as Magnetic ILs (MILs) has been explored. These materials that combine simultaneously ionic liquid properties and magnetic properties, in particular, the response to strong magnetic fields, were firstly reported by Hayashi and Hamaguchi in 2004. [8,9] MILs have a broad range of applications in chemical reactions and separation processes, in electrochemical and medical devices, as solvents in the polymerization of conducting polymers and as carrier liquids to produce magnetic fluids. [10,11] MILs containing iron as well as other paramagnetic ions including transition metals, such as cobalt(II), manganese(II) and some lanthanides, such as gadolinium(III) and terbium(III), have been reported. [10,12–15] However, their toxicity is a matter of concern. Several MILs based on choline derivative structures as cations and paramagnetic metal based anions have been explored to modulate their toxicity.[14,16] Choline is a quaternary ammonium cation with a hydroxyethyl group that plays a critical role in the human body system. This essential nutrient needed for the synthesis of the acetylcholine neurotransmitter, plays a fundamental role in cell membrane signalling among other important functions, and can be synthesized endogenously or acquired through diet. [17] The hydroxyethyl group present in the choline structure is one of the reasons associated with the low toxicity of these compounds. [18] In this work, magnetic organic salts immobilized in MSNs, based on two different choline derivative structures as cations and $[MnCl_3]^-$, $[GdCl_4]^-$ and $[TbCl_4]^-$ as anions, were prepared. All nanomaterials were fully characterized, and their cytotoxicity evaluated in four different cell lines, 3T3, Caco-2, HepG2 and 293T.

[a] LAQV-REQUIMTE, Faculdade de Ciências e Tecnologia, Universidade Nova de Lisboa, Campus da Caparica, 2829-516 Caparica, Portugal;
[b] ITQB NOVA - Instituto de Tecnologia Química e Biológica António Xavier, Avenida da República, Estação Agronómica Nacional, 2780-157 Oeiras
[c] Centro de Química de Évora, LAQV-REQUIMTE, Instituto de Investigação e Formação Avançada, Departamento de Química, Escola de Ciências e Tecnologia, Universidade de Évora, Colégio Luís António Verney, 7000-671 Évora, Portugal
[d] MARE—Marine and Environmental Sciences Centre, Politécnico de Leiria, Avenida Porto de Pesca, 2520-630 Peniche, Portugal;
[e] Centro de Química Estrutural, Instituto Superior Técnico, Universidade de Lisboa, Avenida Rovisco Pais, 1049-001 Lisboa, Portugal;
[f] * Correspondence: l.branco@fct.unl.pt, s.gago@fct.unl.pt

Electronic Supplementary Information (ESI) available: [details of any supplementary information available should be included here]. See DOI: 10.1039/x0xx00000x

2. Results and discussion

2.1. Synthesis of magnetic organic salts based on choline derivatives.

Using optimized alkylation methods, a set of choline derivative cations were synthesized from three different amines. From these compounds, two selected chloride-based organic salts, $[N_{1,1,4,C2OH}][Cl]$ and $[N_{1,1,4,C3OH}][Cl]$, were used to carry out metal complexation reactions with two different lanthanides, Gadolinium(III) and Terbium(III), and one transition metal, Manganese(II), in order to obtain the organic salts, as illustrated in Scheme 1.

Some physical properties of these metal organic salts, such as their physical state and thermal properties (melting and decomposition temperatures) were evaluated (Table 1). All compounds were obtained as solids materials with transition temperatures higher than 100 °C. For $[N_{1,1,4,C3OH}]$ based salts, no melting point was found and only decomposition temperatures could be measured.

Typically, organic salts based on biocompatible choline derivatives showed low toxicity. However, their combination with metals can increase this parameter. When coordinated with a large linear molecule, the metal toxicity is reduced since the metal is trapped. In this work, the metal organic salts were immobilized in MSNs and the impact of this immobilization in their toxicity profile evaluated.

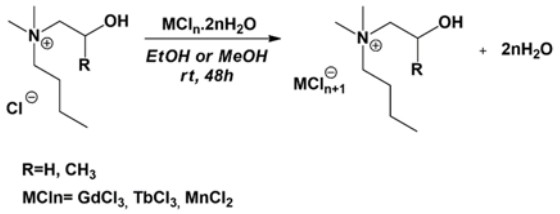

Scheme 1. Schematic synthetic step of the magnetic organic salts based on choline derivative cations.

Table 1. Physical and thermal properties of magnetic organic salts

Cation	Anion	Physical State	Tm [Td] [a] (°C)
$[N_{1,1,4,C2OH}]$	$[GdCl_4]$	White Solid	[118]
	$[TbCl_4]$	White Solid	[115]
	$[MnCl_3]$	Pink Solid	[191]
$[N_{1,1,4,C3OH}]$	$[GdCl_4]$	Yellow Solid	148
	$[TbCl_4]$	Yellow Solid	155
	$[MnCl_3]$	Yellow Solid	132

[a] Melting temperature (Tm) and decomposition temperature (Td) was determined on Electrothermal Melting Point Apparatus.

2.2. Synthesis and functionalization of MSNs

Two sets of mesoporous silica nanoparticles functionalized with magnetic organic salts were developed. The optimized synthetic methodology to obtain these materials comprises four major steps as shown in Scheme 2. Alkoxysilane precursors Si-DMAE and Si-DMAP, analogues of the $[N_{1,1,4,C2OH}]$ and $[N_{1,1,4,C3OH}]$ cations with a small difference of a propyl chain instead of a butyl chain (see Schemes 1 and 2), were synthesized by performing two amine alkylation reactions between (3-chloropropyl)triethoxysilane and two different amines, 2-dimethylaminoethanol (DMAE) or 1-dimethylamino-2-propanol (DMAP). Mesoporous silica nanoparticles precursors, MSN-A and MSN-B, were prepared based on a well-stablished methodology already described in the literature.[19] The CTAB surfactant was used as a template and its removal was performed using acidic ethanol in order to reduce nanoparticle aggregation. Then, the surface silanol groups were functionalized with the alkoxysilane derivates to obtain MSN-Si-

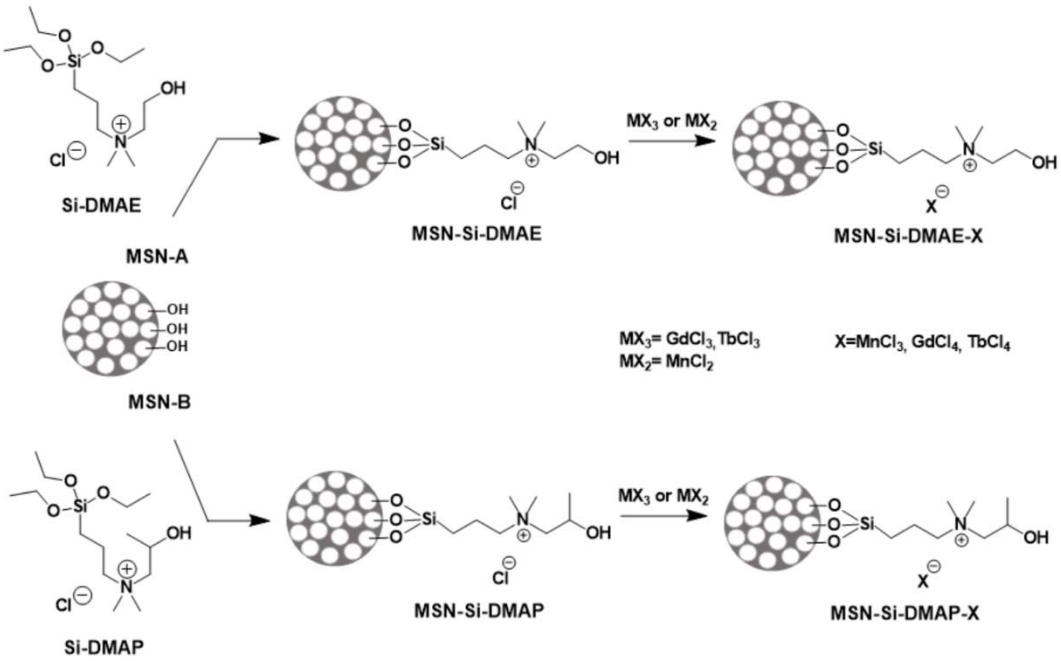

Scheme 2. Schematic illustration of the preparation process of silica mesoporous nanoparticles.

DMAE and MSN-Si-DMAP containing the choline derivatives as cations and chloride as anions. Finally, MSNs containing $[MnCl_3]^-$, $[GdCl_4]^-$ and $[TbCl_4]^-$ anions were obtained by reaction of the chloride ions with the corresponding metal chlorides. These final materials were characterized by several techniques: ^{1}H-NMR (proton nuclear magnetic resonance), FT-IR (Fourier-transformed infrared), EA (elemental analysis), ICP-MS (inductively coupled plasma mass spectrometry), TEM (transmission electron microscopy), TGA (thermogravimetric analysis), N_2 adsorption, XRD (X-ray diffraction) and DLS (dynamic light scattering).

The successful functionalization of MSNs with choline derivatives was confirmed by ^{1}H-NMR (Figure 1), FT-IR (supplementary information) and elemental analysis. To obtain solution ^{1}H-NMR spectra of MSN-Si-DMAE and MSN-Si-DMAP, the silica matrix was destroyed according to the method described in the literature.[20] The peaks obtained for MSN-Si-DMAE and MSN-Si-DMAP were assigned to the organic salts protons in Figure 1 (A) and (B), respectively. FT-IR spectra of functionalized materials (supporting information, Figure S1, S2 and Table S1) clearly show the typical silica absorption bands at 1095cm^{-1} for MSN-A and 1092cm^{-1} for MSN-B and, also, the presence of Si-DMAE and Si-DMAP chloride salts could be confirmed by the bands associated with C-H bonding vibrations at 1477cm^{-1} and 1400cm^{-1} for MSN-Si-DMAE and 1479cm^{-1} and 1400cm^{-1} for MSN-Si-DMAP.

Elemental analysis indicates 1.50 mmol/g of cation for MSN-Si-DMAE and 1.45 mmol/g of cation for MSN-Si-DMAP (Table 2).

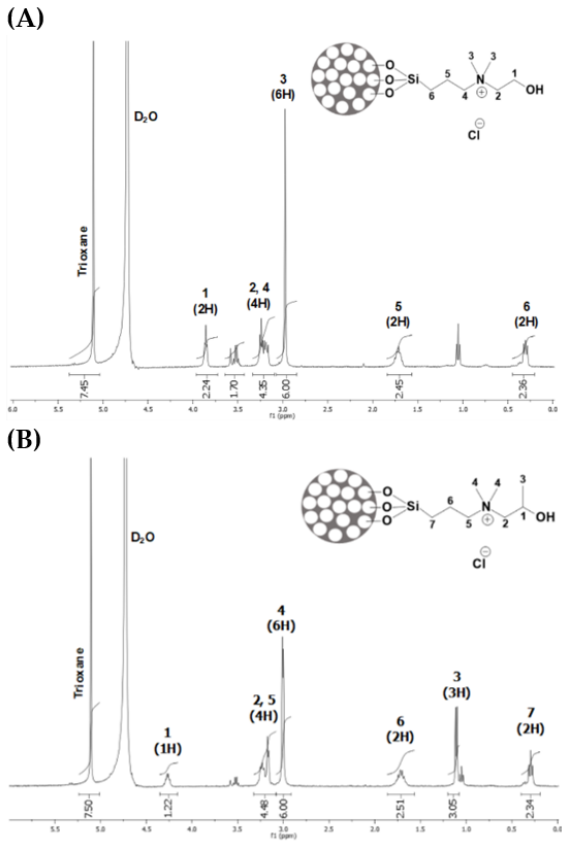

Figure 1. Solution ^{1}H-NMR spectra for (A) MSN-Si-DMAE and (B) MSN-Si-DMAP (in D_2O and NaOH).

Table 2. Cation and metal loadings based on elemental analysis and ICP-MS results

Sample	Cation (mmol/g)	Metal (mmol/g)
MSN-Si-DMAE	1.50	-
MSN-Si-DMAE-Gd	1.50	0.07
MSN-Si-DMAE-Tb	1.35	0.09
MSN-Si-DMAE-Mn	1.47	0.19
MSN-Si-DMAP	1.45	-
MSN-Si-DMAP-Gd	1.42	0.03
MSN-Si-DMAP-Tb	1.31	0.02
MSN-Si-DMAP-Mn	1.43	0.04

The final materials were also characterized by ICP-MS and the results show that metal loadings range from 0.02 mmol/g to 0.19 mmol/g (Table 2). Higher metal loadings were achieved for the Si-DMAE cation which can be related to possible steric effects resulting from the presence of a secondary alcohol in the Si-DMAP cation. Another important piece of information that can be taken from these results is the incomplete complexation reactions between the chloride ions and the metal chlorides. The metal values in percentage per cation unit are in the range of 2.25-13.18%, which means that the majority of the cations are in the MSN structure with chloride as counter ion. The overall amount of loaded organic cation in nanoparticles, which by elemental analysis is around 20% (in mass) for MSN-Si-DMAE and 21% for MSN-Si-DMAP, was confirmed by thermogravimetric analysis. TGA curves, presented in Figure 2 for all studied materials, indicate a 2 to 4% mass loss between 80 and 200 °C, which can be justified by the release of water. TGA curves of MSN-Si-DMAE and MSN-Si-DMAP, presented in Figure 2A and 2B respectively, are similar and show two main mass changes, the first between 200 °C and 290 °C that corresponds to 9% mass loss and another in the 330-500 °C range. Between 200 °C and 500 °C, 20% mass loss for MSN-Si-DMAE and 21.9% for MSN-Si-DMAP were obtained, which is consistent with the organic cations content obtained by elemental analysis. Regarding MSN-Si-DMAE-X and MSN-Si-DMAP-X and the first step, the same behavior of their precursors could be found for most materials and the mass loss is also 9%, although for some materials slightly higher temperatures are required to obtain the same mass loss. Considering now the second mass change, it occurs at higher temperatures than for MSN-Si-DMAE and MSN-Si-DMAP materials. The observed displacements to higher temperatures are due to the presence of metal complexes and their interactions with the organic cations.

2.3. Characterization by transmission electron microscopy, nitrogen adsorption at 77 K and X-ray diffraction

The prepared nanoparticles were characterized according to their morphology and particle size. MSN-A, MSN-B and all metal based nanoparticles were analyzed by transmission electron microscopy (TEM). Nanoparticle images and the average diameter values obtained from TEM can be seen in Figure 3. The images show monodisperse nanoparticles with spherical shape and some aggregation. All nanoparticles presented similar particle average diameter values. Even so, it is possible to

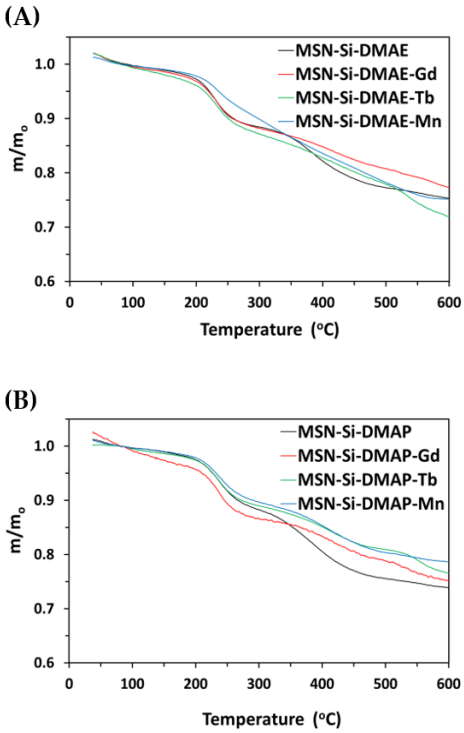

Figure 2. Thermogravimetric analysis of (A) MSN-Si-DMAE and MSN-Si-DMAE-X; (B) MSN-Si-DMAP and MSN-Si-DMAP-X (m_o is the mass at 80 °C).

observe that Si-DMAE-based materials have a very slightly larger diameter than Si-DMAP-based materials.

N_2 adsorption-desorption isotherms determined at 77 K on silica nanoparticles MSN-A and MSN-B are presented respectively in Figure 4A and 4B on the left, together with the representative adsorption-desorption isotherm for each material after functionalization. Considering that no differences could be seen in this scale for the functionalized materials, adsorption isotherms are shown in another scale in the figures on the right for all the functionalized materials. The N_2 adsorption-desorption isotherms were analysed by the BET method using the criteria recommended by Rouquerol *et al*., [21] and subsequently endorsed by IUPAC,[22] and by NLDFT using the Quantachrome software ASiQwin. The results are summarized in Table 3.

As can be seen in Figure 4, the isotherms obtained on MSN-A and MSN-B are type IV of the IUPAC classification,[22] with a well-defined step associated with filling of cylindrical mesopores by capillary condensation. The pore size distributions, inserted into the figures on the left, show that the pore diameter is reasonably uniform in both silica materials. The nitrogen adsorption-desorption isotherms on the nanoparticles are reversible up to a high pressure, and values above 0.9 show a hysteresis cycle that is usually obtained on materials with small size spherical nanoparticles and is associated with capillary condensation in voids between particles. The functionalization did not affect the shape of the hysteresis cycle which was found to be similar for all materials.

Regarding the nitrogen adsorption and condensation in the uniform mesopores, a reduction in the adsorbed amounts was obtained for all the functionalized materials. As expected, functionalized materials present smaller values of specific surface areas and pore volumes, and a decrease in the pore size distributions when compared to the starting materials MSN-A and MSN-B. For the materials with the same organic cation, no significant differences were found for different metals. Nevertheless, the nanomaterials with lanthanides have slightly larger specific surface areas and pore volumes in both series. When the materials with different organic cation and the same metal are compared, larger values can be observed for MSN-Si-DMAP-X materials. It is noticeable in the nitrogen adsorption isotherms on MSN-Si-DMAP-X that a pore filling step is still perceptible and displaced to a lower relative pressure due to the decrease of pore size as obtained from NLDFT. Regarding MSN- Si-DMAE-Gd and MSN-Si-DMAE-Tb, the mean pore size is maintained, while in the case of MSN-Si-DMAE-Mn the slightly larger mean pore size results from the disappearance of pores of smaller size as found in the pore size distribution. All the nitrogen adsorption results are consistent with the smaller %metal/cation found, in each series, for lanthanides in comparison with Mn, and the smaller %metal/cation for all

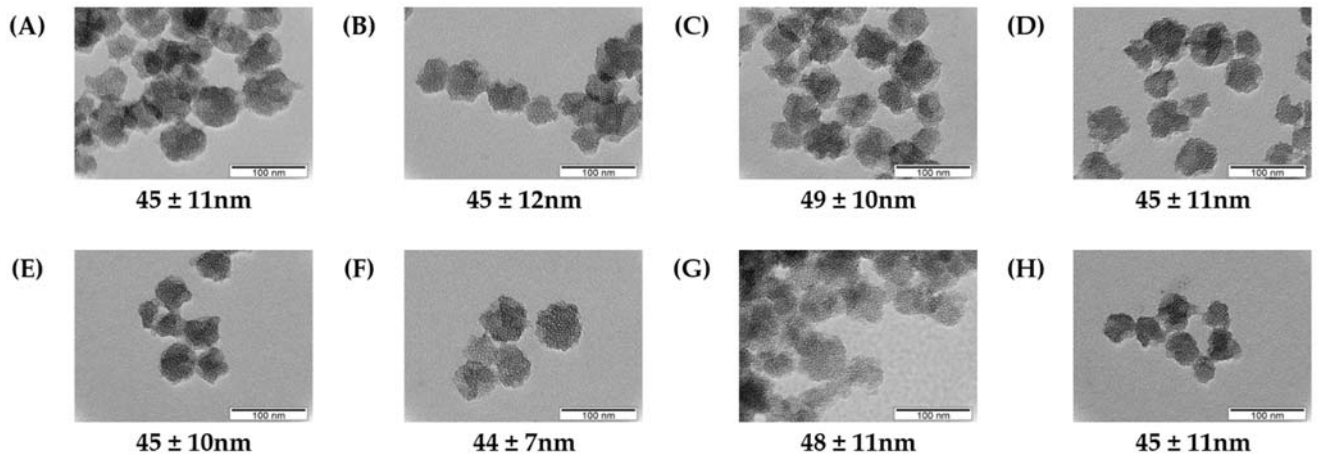

Figure 3. Transmission electron microscopy images and mean diameter ± SD of (A) MSN-A; (B) MSN-Si-DMAE-Gd; (C) MSN-Si-DMAE-Tb; (D) MSN-Si-DMAE-Mn; (E) MSN-B; (F) MSN-Si-DMAP-Gd; (G) MSN-Si-DMAP-Tb; (H) MSN-Si-DMAP-Mn.

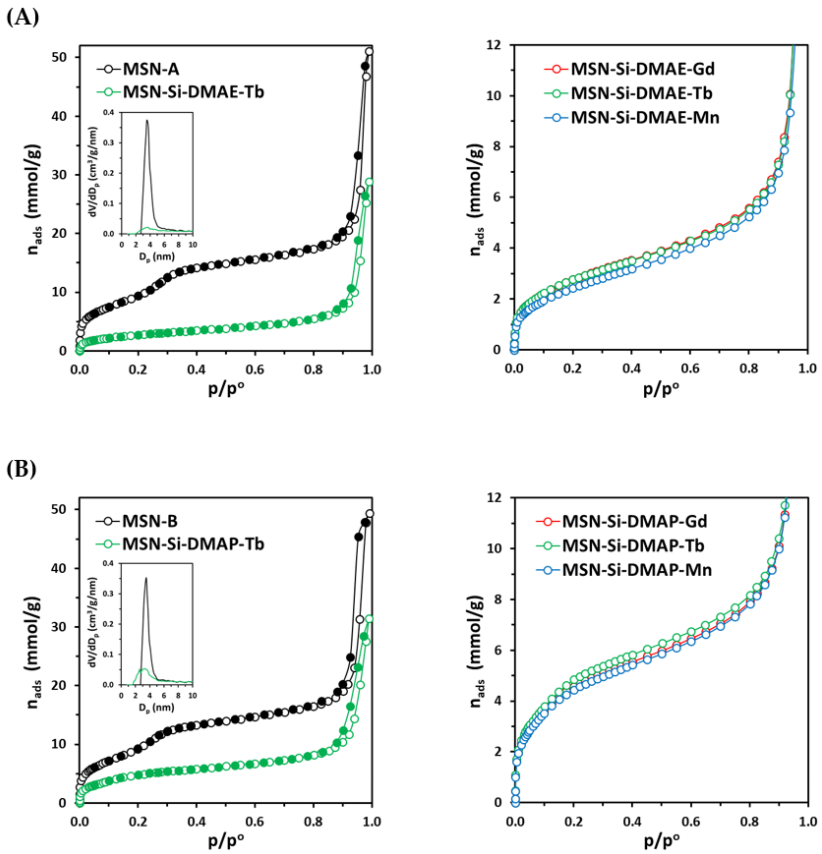

Figure 4. Nitrogen adsorption isotherms determined at 77 K on (A) MSN-A and MSN-Si-DMAE-X; (B) MSN-B and MSN-Si-DMAP-X. NLDFT pore size distributions are inseted in the figures on the left.

Table 3. Textural characteristics of the mesoporous silica nanoparticles obtained by analysis of the N_2 adsorption isotherms determined at 77 K

Sample	A_{BET} (m^2/g)	D_p (nm)	V_p (cm^3/g)
MSN-A	743	3.54	0.44
MSN-Si-DMAE-Gd	228	3.54	0.08
MSN-Si-DMAE-Tb	228	3.54	0.08
MSN-Si-DMAE-Mn	200	3.78	0.07
MSN-B	719	3.54	0.39
MSN-Si-DMAP-Gd	382	3.18	0.14
MSN-Si-DMAP-Tb	400	3.18	0.15
MSN-Si-DMAP-Mn	371	3.18	0.13

A_{BET} – specific surface area obtained by the BET method in the p/p° range 0.045-0.12 for all; D_p – pore diameter obtained from the NLDFT pore size distributions; V_p – cumulative pore volume corresponding to 8 nm obtained from the NLDFT pore size distributions.

metals found for MSN-Si-DMAP-X. Thus, more space in pores is available since chloride counter ions occupy a smaller volume than the metal complexes.

As can be seen in Figure 5, the X-ray diffraction patterns of MSN-A and MSN-B have a main peak in the low-angle region at around 2° (2θ), and another with a much lower intensity at around 4° (2θ), indicating some ordering of the pores with a reasonably uniform pore size. The main peak is broader, less intense and corresponds to a d-spacing larger than usually obtained for MCM-41 and MCM-48 silicas with similar average pore diameters, consistent with a less ordered arrangement of the pores inside such small nanoparticles. All the functionalized materials present a broad peak also at around 2° (2θ), although with a lower intensity than those of the starting silica materials, indicating that some ordered mesopores remain after functionalization. Consistent with the nitrogen adsorption studies and the smaller %metal/cation in MSN-Si-DMAP-X, the peak is slightly better resolved and more intense for MSN-Si-DMAP-X materials than for MSN-Si-DMAE-X.

2.4. Nanoparticles' Colloidal Stability

The prepared MSNs, before and after functionalization, were suspended in water by sonication and their colloidal stability monitored by dynamic light scattering (DLS). Hydrodynamic diameter and zeta potential values were measured for all nanomaterials and the results are summarized in Table 4. As can be seen, hydrodynamic diameters are in the range of 107-204nm, with an average polydispersity index of 0.36. As is well known, smaller nanoparticles have a higher surface energy which makes the particles more prone to aggregate, in order to lower the energy of the system.[23] According to TEM images, prepared nanoparticles have an average size in the range of 45-49nm. Their small size can lead to an aggregation phenomenon, proved by their hydrodynamic diameter values obtained by DLS measurements. Non-functionalized nanoparticles MSN-A and MSN-B have much higher values of hydrodynamic diameter than functionalized materials. This effect can be related to a

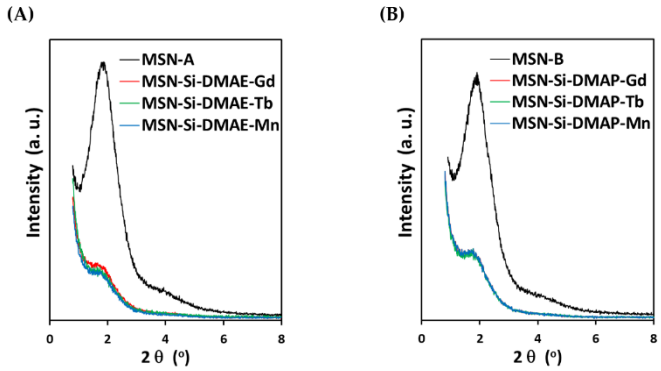

Figure 5. X-ray diffraction patterns of (A) MSN-A and MSN-Si-DMAE-X; (B) MSN-B and MSN-Si-DMAP-X.

major tendency to aggregate. These materials also presented a negative zeta potential (-9.90mV and -5.36mV) due to the negatively charged terminal silanol groups present at the nanoparticle surface and the pH used in this study. When MSN-A and MSN-B are functionalized with DMAE and DMAP structures, the values of hydrodynamic diameters decrease, and their zeta potential values change from negative to positive due to the positive charge associated to choline derivatives scaffolds. When metal complexes are introduced in the nanoparticles, slightly lower values of zeta potential are obtained. Higher values of hydrodynamic diameters and zeta potentials were obtained for MSN-Si-DMAP and MSN-Si-DMAP-X nanoparticles. High zeta potential values obtained for all prepared nanoparticles indicate the high colloidal stability of these materials in water suspensions. Moreover, PDI values indicate that these materials are monodisperse which is in correlation with the TEM results.

Figure 6 shows the time evolution of hydrodynamic diameter distributions of the prepared nanoparticle suspensions. It can be observed that colloidal suspensions with DMAE-based nanoparticles are more stable than those with DMAP-based nanoparticles. Also, the shape and value of hydrodynamic diameter curves are maintained for DMAE-based nanomaterials. This can be related to the presence of a secondary alcohol in the DMAP structure since the presence of a branched structure is usually responsible for the decrease of attractive forces between molecules. Also, the presence of metal complexes seems to have some effect on the stability of the nanoparticles. As can be observed, MSN-Si-DMAE-X and MSN-Si-DMAP-X present hydrodynamic diameter distribution curves with a tendency to change significantly over time. In contrast, MSN-Si-DMAE and MSN-Si-DMAP have distribution curves with more conserved shapes and values. This effect seems to be more evident for DMAP-based nanoparticles. These conclusions are in agreement with the results obtained for hydrodynamic diameters and zeta potentials.

2.5. Cytotoxicity

Cytotoxicity of magnetic organic salts and prepared mesoporous silica nanoparticles was evaluated on 3T3, 293T, HepG2 and Caco-2 cells after 24 h treatment. All compounds were tested at a maximum concentration of 100 µg/mL. The cells viability was estimated by the MTT assay and the results are presented in the next sections.

2.5.1. Choline derivatives magnetic organic salts

The effects of two choline derivative salts with chloride and metal complexes as anions on studied cells' viability are presented in Figure 7. The starting metal chlorides were also studied. It is possible to observe that the majority of the compounds did not induced any cytotoxicity on the cell lines studied compared to control situation. Even so, there are some exceptions that can be highlighted. Manganese-based salts, $[N_{1,1,4,C2OH}][MnCl_3]$ and $[N_{1,1,4,C3OH}][MnCl_3]$, as well as $MnCl_2.4H_2O$, reduced significantly the viability of 3T3 cells (63.00%, 73.76% and 67.21% of viable cells, respectively) compared with control situation. In 293T cells, when compared with control, only the synthesized salt $[N_{1,1,4,C3OH}][MnCl_3]$ and $MnCl_2.4H_2O$ showed to significantly reduce the cells viability in more than 35% and 40%, respectively. For these cells, some prepared compounds and also gadolinium and terbium chlorides presented cells viability higher than 100%, which can suggest that these magnetic salts may enhance the mitochondrial activity. $[N_{1,1,4,C3OH}][TbCl_4]$ salt was the only prepared compound that significantly reduced the HepG2 and

Table 4. Hydrodynamic diameter and zeta potential of the final materials obtained in water by DLS (mean ±SD)

Sample	Average hydrodynamic diameter (nm)	Polydispersity index (PDI)	Zeta Potential (mV)	pH
MSN-A	204 ± 28.30	0.38 ± 0.04	-9.90 ± 3.12	5.07
MSN-Si-DMAE	107 ± 2.63	0.35 ± 0.03	+49.46 ± 1.72	4.65
MSN-Si-DMAE-Gd	110 ± 0.76	0.29 ± 0.02	+43.16 ± 1.62	4.04
MSN-Si-DMAE-Tb	123 ± 2.52	0.40 ± 0.03	+46.40 ± 1.36	4.06
MSN-Si-DMAE-Mn	125 ± 0.76	0.34 ± 0.03	+45.06 ± 1.77	4.00
MSN-B	193 ± 1.89	0.42 ± 0.06	-5.36 ± 2.21	4.15
MSN-Si-DMAP	135 ± 1.82	0.33 ± 0.08	+59.16 ± 1.24	4.17
MSN-Si-DMAP-Gd	125 ± 5.60	0.37 ± 0.05	+48.10 ± 1.08	3.93
MSN-Si-DMAP-Tb	137 ± 0.61	0.34 ± 0.12	+43.76 ± 1.72	4.06
MSN-Si-DMAP-Mn	149 ± 2.84	0.42 ± 0.12	+49.58 ± 1.21	4.00

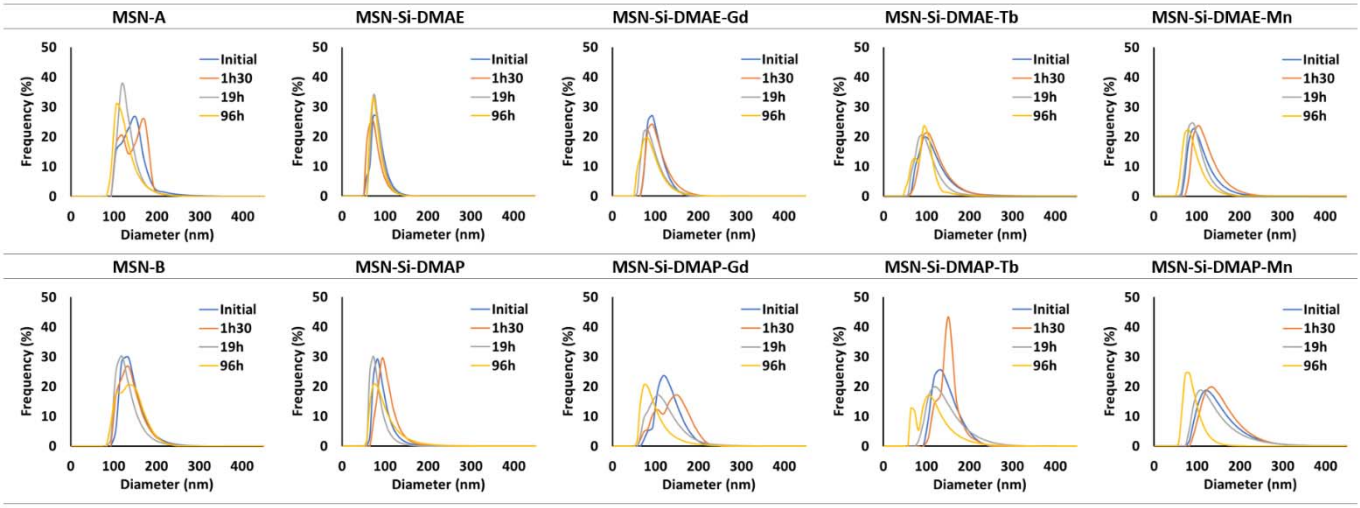

Figure 6. Time evolution of hydrodynamic diameter distributions of the prepared nanoparticles suspensions in water.

Caco-2 cells' viability compared with to control situation. Also, $GdCl_3.6H_2O$ and $MnCl_2.4H_2O$ induced a reduction effect on Caco-2 cells' viability when compared with control situation. In general, the compounds based on cations $[N_{1,1,4,C2OH}]$ and $[N_{1,1,4,C3OH}]$ exhibited a similar behavior.

2.5.2. Mesoporous Silica Nanoparticles

The effects of all prepared nanoparticles on studied cells viability are shown in Figure 8. Concerning to prepared nanomaterials, the cytotoxicity of the two set of nanoparticles based on DMAE and DMAP scaffolds and their precursors were evaluated. In 3T3 cells, for the first set of materials, it is possible to observe that the nanoparticles before and after functionalization, MSN-A and MSN-Si-DMAE, significantly reduce the cells viability in more than 20% (79.96% and 72.32% of viable cells, respectively) when compared with control. Regarding to the metal-based materials, only MSN-Si-DMAE-Tb showed to reduce the cells viability in these cell lines. Regarding to the second set of nanoparticles, MSN-B also showed to reduce the cells viability (52.11% of viable cells) and all metal-based materials showed to be responsible for a significant reduction of cells viability compared to control situation. In this

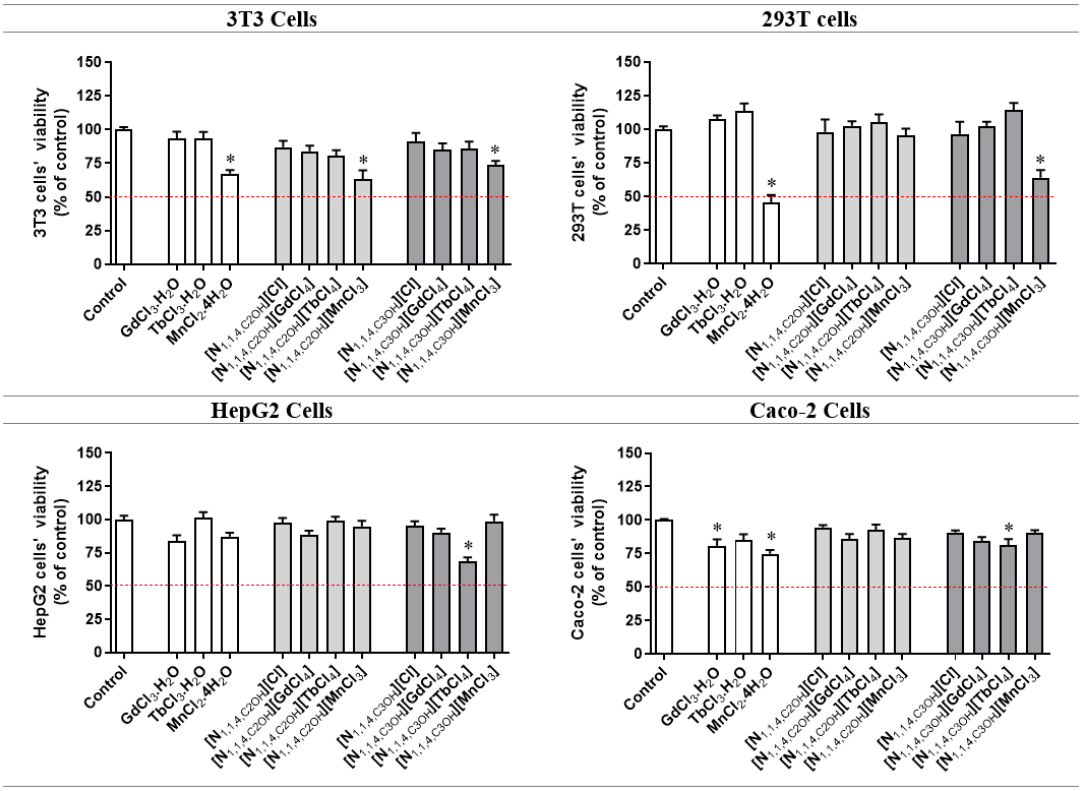

Figure 7. Cytotoxicity of magnetic organic salts (100 µg/ mL) on 3T3, 293T, HepG2 and Caco-2 cells after treatment for 24 h. Values represent mean ± standard error of the mean (SEM) of at least three independent experiments carried out in triplicate. Symbols represent significant differences (ANOVA, Dunnett's test, $p < 0.05$) when compared to: *control.

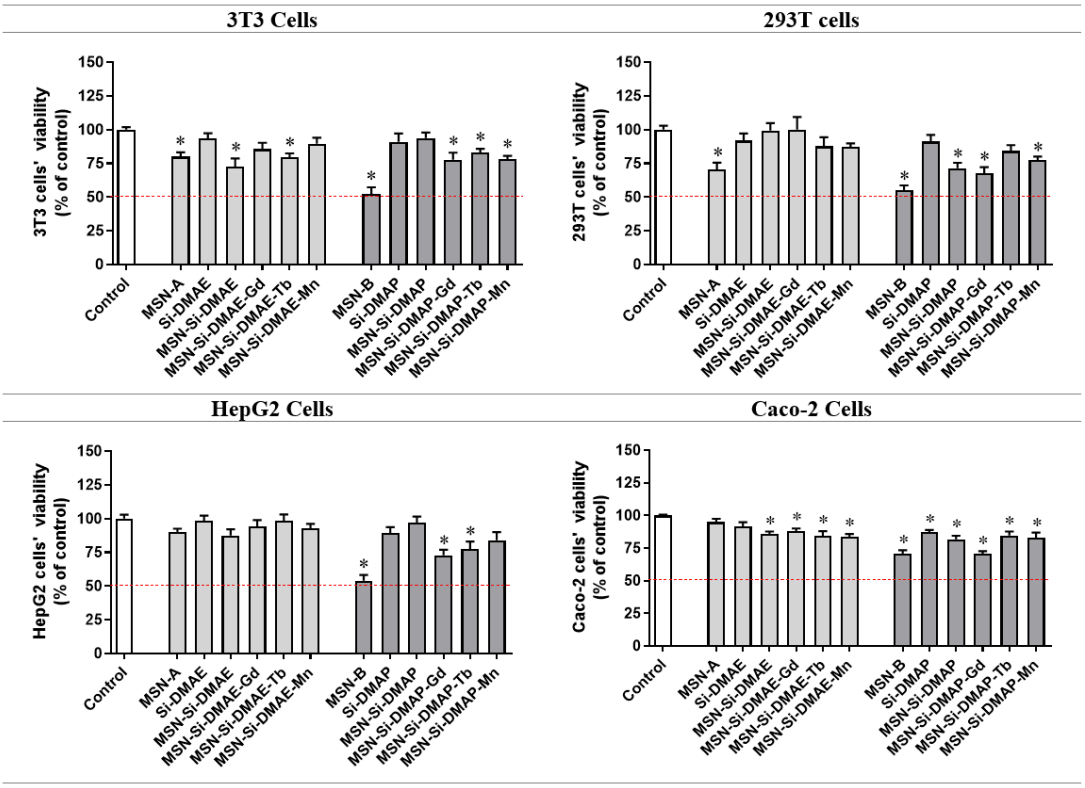

Figure 8. Cytotoxicity of prepared mesoporous silica nanoparticles (100 µg/ mL) on 3T3, 293T, HepG2 and Caco-2 cells after treatment for 24 h. Values represent mean ± standard error of the mean (SEM) of at least three independent experiments carried out in triplicate. Symbols represent significant differences (ANOVA, Dunnett's test, $p < 0.05$) when compared to: *control.

case, a range of 77.65-83.09% of viable cells was achieved. In 293T cells, among DMAE set only MSN-A presented a significative reduction of cells viability in almost 30% in comparison to control. For DMAP set, almost all induced the cells viability reduction, with the exceptions being Si-DMAP and MSN-Si-DMAP-Tb. DMAE-based materials and their precursors do not seem to have any effect in HepG2 cells. MSN-B, MSN-Si-DMAP-Gd and MSN-Si-DMAP-Tb, on the contrary, induced a cells viability reduction of 46.05%, 27.85% and 22.5%, respectively, compared to control situation. Finally, almost all induced cytotoxicity in Caco-2 cells (70.50-87.88% of viable cells) and only MSN-A and Si-DMAE did not exhibited a cytotoxic effect. As can be seen, the DMAP-based materials and its precursors seem to induce an effect more marked on the cells viability than DMAE-based materials.

2.5.3. Choline derivatives magnetic organic salts vs MSNs containing magnetic organic salts analogues

A final comparison between the cytotoxicity of metal organic salts and their analogues immobilized in mesoporous silica nanoparticles is summarized in Figure 9.

In general, no significant differences could be found between metal organic salts and their analogues immobilized in MSNs. Only a few examples can be highlighted in 3T3, 293T and Caco-2 cells. In 3T3 cells, only $[N_{1,1,4,C2OH}][MnCl_3]$ and MSN-Si-DMAE-Mn showed significant differences. In this case, the immobilized analogue exhibited a smaller cytotoxic effect compared with the metal organic salt. In 293T cells, two pairs ($[N_{1,1,4,C3OH}][GdCl_4]$/MSN-Si-DMAP-Gd and $[N_{1,1,4,C3OH}][TbCl_4]$/MSN-Si-DMAP-Tb), displayed significant differences between the effect of the two systems in cells viability. For both, the nanoparticles presented a higher cytotoxic effect than the metal organic salts. In Caco-2 cells, MSN-Si-DMAP-Gd nanoparticles induced higher cytotoxic effect than $[N_{1,1,4,C3OH}][GdCl_4]$ in cells viability.

3. Experimental Section

3.1. Chemicals

All reagents used in the synthesis of magnetic salts and preparation of nanoparticles namely, Pluronic F 127 (BASF), n-cetyltrimethylammonium bromide (CTAB, $(C_{16}H_{33})N(CH_3)_3]Br$, Sigma-Aldrich), Triethanolamine (TEA, $N(C_2H_5O)_3$, Alfa Aesar), Tetraethyl orthosilicate (TEOS, $Si(OC_2H_5)_4$, Aldrich, 98%), (3-chloropropyl)triethoxysilane ($Cl(CH_2)_3Si(OCH_3)_3$, TCI, >97%), dimethyl(2-hydroxyethyl)amine (Aldrich), dimethyl(2-hydroxypropyl)amine (Aldrich), Gadolinium (III) Chloride Hexahydrate ($GdCl_3.6H_2O$, Alfa Aesar), Terbium (III) Chloride Hexahyhdrate ($TbCl_3.6H_2O$, Aldrich, trace metal basis), Manganese (II) Chloride Tetrahydrate ($MnCl_2.4H_2O$, Alfa Aesar) and 1-Chlorobutane (Sigma-Aldrich, 99%) were purchased from chemical suppliers and used without further purification.

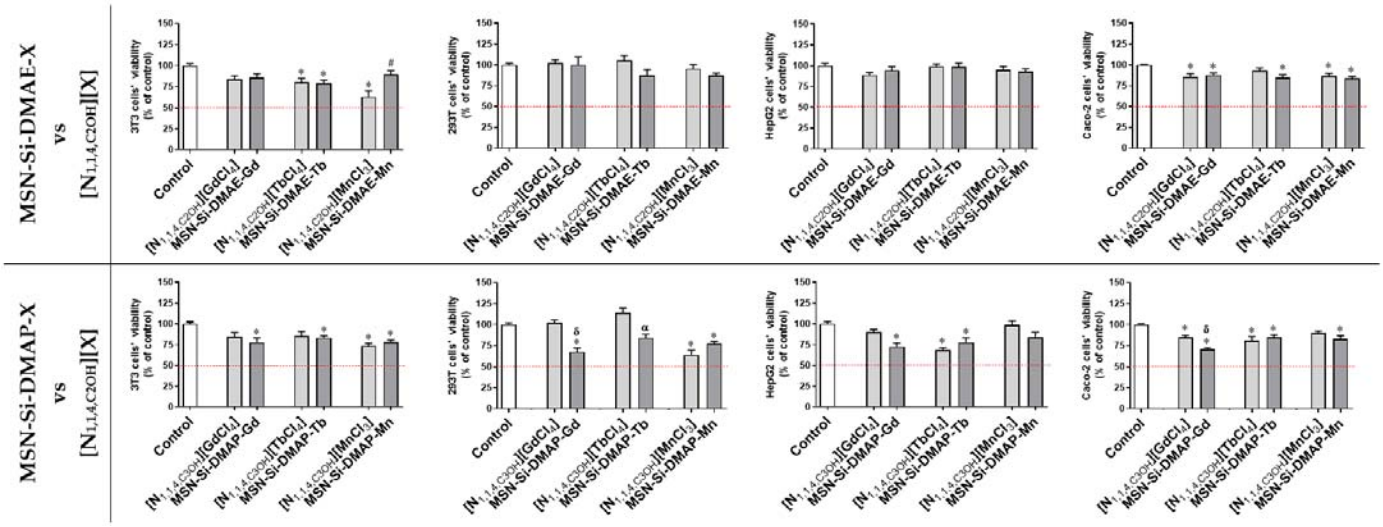

Figure 9. Cytotoxicity of choline derivative magnetic salts (100 µg/ mL) on 3T3, 293T, HepG2 and Caco-2 cells after treatment for 24 h. Values represent mean ± standard error of the mean (SEM) of at least three independent experiments carried out in triplicate. Symbols represent significant differences (ANOVA, Dunnett's test, $p < 0.05$) when compared to: *control, #[$N_{1,1,4,C2OH}$][$MnCl_3$], δ[$N_{1,1,4,C3OH}$][$GdCl_4$], α[$N_{1,1,4,C3OH}$][$TbCl_4$].

3.2.Synthesis of magnetic organic salts

Synthetic general procedure: The metal chloride hydrated ($MCl_n.2nH_2O$) was added to an ethanolic solution of choline derivative salt ([$N_{1,1,4,C2OH}$][Cl] or [$N_{1,1,4,C3OH}$][Cl]) under constant stirring. The reaction mixture was stirred at room temperature for 48 h and then the solvent was evaporated. The final solid was dried under vacuum.

3.2.1. Synthesis of N-butyl-N-hydroxyethyl-N,N-dimethylammonium tetrachlorogadolinate (III) [$N_{1,1,4,C2OH}$][$GdCl_4$]

[$N_{1,1,4,C2OH}$][Cl] (0.20 g, 1.35 mmol); $GdCl_3.6H_2O$ (0.50 g, 1.36 mmol); Yield: quantitative; white solid; FTIR (KBr), $\bar{\upsilon}$ (cm^{-1}) = 3425, 2964-2878, 1625, 1475, 1083, 920. Elemental analysis calcd (%) for $C_8H_{20}NOGdCl_4.0.5H_2O$ (454.35 $g.mol^{-1}$): C 21.15, N 3.08, H 5.67; found: C 21.32, N 3.02, H 5.50.

3.2.2. Synthesis of N-butyl-N-hydroxypropyl-N,N-dimethylammonium tetrachlorogadolinate (III) [$N_{1,1,4,C3OH}$][$GdCl_4$]

[$N_{1,1,4,C3OH}$][Cl] (0.26 g, 1.32 mmol); $GdCl_3.6H_2O$ (0.49 g, 1.30 mmol) Yield: quantitative; yellow solid; FTIR (KBr), $\bar{\upsilon}$ (cm^{-1}) = 3351, 1634, 1476, 1081, 960. Elemental analysis calcd (%) for $C_9H_{22}NOGdCl_4.0.5H_2O$ (468.38 $g.mol^{-1}$): C 23.08, N 2.99, H 4.96; found: C 22.59, N 3.07, H 4.90.

3.2.3. Synthesis of N-butyl-N-hydroxyethyl-N,N-dimethylammonium tetrachloroterbate (III) [$N_{1,1,4,C2OH}$][$TbCl_4$]

[$N_{1,1,4,C2OH}$][Cl] (0.30 g, 2.06 mmol); $TbCl_3.6H_2O$ (0.77 g, 2.07 mmol); Yield: quantitative; white solid; FTIR (KBr), $\bar{\upsilon}$ (cm^{-1}) = 3370, 2965-2876, 1633, 1486, 1131, 1084, 1051, 976, 920. Elemental analysis calcd (%) for $C_8H_{20}NOTbCl_4.2.5H_2O$ (492.28 $g.mol^{-1}$): C 19.53, N 2.85, H 5.13; found: C 19.53, N 2.74, H 5.03.

3.2.4. Synthesis of N-butyl-N-hydroxypropyl-N,N-dimethylammonium tetrachloroterbate (III) [$N_{1,1,4,C3OH}$][$TbCl_4$]

[$N_{1,1,4,C3OH}$][Cl] (0.26 g, 1.32 mmol); $TbCl_3.6H_2O$ (0.46 g, 1.24 mmol); Yield: quantitative; yellow solid; FTIR (KBr), $\bar{\upsilon}$ ($cm^{-1)}$ = 3379, 2971, 1636, 1476, 1143-1077, 990, 947. Elemental analysis calcd (%) for $C_9H_{22}NOTbCl_4.2H_2O$ (497.09 $g.mol^{-1}$): C 21.74, N 2.82, H 5.28; found: C 22.15, N 2.85, H 6.00.

3.2.4. Synthesis of N-butyl-N-hydroxyethyl-N,N-dimethylammonium trichloromanganese (II) [$N_{1,1,4,C2OH}$][$MnCl_3$]

[$N_{1,1,4,C2OH}$][Cl] (0.50 g, 3.43 mmol); $MnCl_2.4H_2O$ (0.68 g, 3.44 mmol); Yield: quantitative; pink solid; FTIR (KBr), $\bar{\upsilon}$ (cm^{-1}) = 3440 2964, 1615, 1469, 1086, 977, 922. Elemental analysis calcd (%) for $C_8H_{20}NOMnCl_3.3H_2O$ (361.64 $g.mol^{-1}$): C 26.57, N 3.87, H 7.26; found: C 26.40, N 3.73, H 6.68.

3.2.5. Synthesis of N-butyl-N-hydroxypropyl-N,N-dimethylammonium trichloromanganase (II) [$N_{1,1,4,C3OH}$][$MnCl_3$]

[$N_{1,1,4,C3OH}$][Cl] (0.26 g, 1.31 mmol); $MnCl_2.4H_2O$ (0.27 g, 1.30 mmol); Yield: quantitative; yellow solid; FTIR (KBr), $\bar{\upsilon}$ (cm^{-1}) = 3425, 2967, 1633, 1485, 1148, 1011, 994, 908. Elemental analysis calcd (%) for $C_9H_{22}NOMnCl_3.H_2O$ (321.61): C 33.61, N 4.36, H 6.91; found: C 33.25, N 4.45, H 7.36.

3.3. Synthesis of Mesoporous Silica Nanoparticles (MSNs)

3.3.1. Synthesis of MSNs

MSNs used in this work were prepared based on a previously reported method described by Bouchoucha.[19] CTAB (1.33 g), F-127 (5.36 g) and TEA (31.3 g) were added to a Teflon vessel and were dissolved in ethanol absolute (114 mL) and water (250 mL). The final solution was placed under constant stirring overnight. TEOS (5.12 mL) was then added at room temperature under vigorous constant stirring and left for 1 min. The mixture was then left under static conditions. After 24h, ethanol (200

mL) was added and the colloidal solution was centrifuged (18 000 rpm for 15 minutes). The final product was washed with water twice and then dried overnight at 70 ºC. Finally, in order to extract the surfactant, the nanoparticles were mixed with acidic ethanol (0.1 M) and kept under constant stirring and reflux overnight. The final nanoparticles were washed with ethanol three times and dried overnight at 70 ºC (MSN-A - 1.51 g and MSN-B - 2.04g). FTIR $_{MSN-A}$ (KBr): $\bar{\upsilon}$ (cm-1) = 3448, 2959-2925, 1637, 1400, 1089, 965. FTIR $_{MSN-B}$ (KBr): $\bar{\upsilon}$ = 3449, 2926, 1637, 1400, 1088, 965.

3.3.2. Synthesis of precursors Si-DMAE and Si-DMAP

General procedure: (3-chloropropyl)triethoxysilane and the selected amine (DMAE or DMAP) were added to a round-bottomed flask. The reaction mixture was stirred for 24h at 80 °C. The final mixture was then washed with diethyl ether and dried under vacuum to give the final product.

Si-DMAE: (3-chloropropyl)triethoxysilane (4.05 mL); DMAE (1.69 mL); Yield: 4.78g, 86%; ^{1}H-NMR (400MHz, $CD_3(SO)_2$): δ (ppm) = 3.78 (m, 8H), 3.39 (m, 4H), 3.09 (s, 6H), 1.71 (m, 2H), 1.16 (m, 9H), 0.52 (m, 2H).

Si-DMAP: (3-chloropropyl)triethoxysilane (1.18 mL); DMAP (2.8 mL); Yield: 2.76 g, 83%; ^{1}H-NMR (400MHz, $CDCl_3$): δ (ppm) = 4.54 (m, 1H), 3.83 (q, ^{3}J(H,H)=6.8 Hz, 6H), 3.55 (m, 4H), 3.39 (d, ^{3}J(H,H)=5.2 Hz, 6H), 1.87 (m, 2H), 1.31 (d, ^{3}J(H,H)=6.0 Hz, 9H), 1.23 (t, ^{3}J(H,H)=7.0 Hz, 2H), 0.64 (m, 2H).

3.3.3. MSNs functionalization with Si-DMAE and Si-DMAP precursors

General procedure: Prepared MSNs (MSN-A and MSN-B) and ethanol (20mL) were added to a round-bottomed flask. To the resultant suspension was added the precursor (Si-DMAE or Si-DMAP). The reaction was kept under reflux with constant stirring for 24h at 100 °C. The reaction mixture was centrifuged (5000 rpm, 15 minutes) and then washed with ethanol four times. Finally, the final product was dried overnight at 80 °C to give the final product.

MSN-Si-DMAE: MSN-A (1.015 g); Si-DMAE (0.950 g); MSN-Si-DMAE (1.29 g); ^{1}H-NMR (400MHz, D_2O+NaOH): δ (ppm) = 3.86 (t, ^{3}J(H,H)=5.6 Hz, 2H), 3.21 (m, 4H), 2.97 (s, 6H), 1.70 (m, 2H), 0.28 (m, 2H); FTIR (KBr): $\bar{\upsilon}$ (cm^{-1})= 3422, 2970, 1638, 1477, 1400, 1095, 959; Elemental analysis (%) found: C 11.35, N 2.30, H 2.34.

MSN-Si-DMAP: MSN-B (1.032 g); Si-DMAP (1.002 g); Yield: MSN-Si-DMAP (1.21 g). ^{1}H-NMR (400MHz, D_2O+NaOH): δ (ppm) = 4.27 (m, 1H), 3.23 (m, 2H), 3.17 (m, 2H), 3.01 (s, 6H), 1.70 (m, 2H), 1.10 (d, ^{3}J(H,H)=6.4 Hz, 3H), 0.29 (m, 2H); FTIR (KBr): $\bar{\upsilon}$ (cm^{-1})= 3422, 2920, 1637, 1479, 1400, 1092, 958; Elemental analysis (%) found: C 12.15, N 2.28, H 2.71.

3.3.4. Synthesis of supported metal organic salts analogues

General procedure: Functionalized materials (MSN-Si-DMAE and MSN-Si-DMAP) and ethanol were added to a flask. To the resultant suspension, $MCl_n.2nH_2O$ was added. The reaction mixture was stirred at room temperature for one week and then the product was washed with ethanol (three times). Finally, the solid was dried overnight at 80 °C to give the final product.

MSN-Si-DMAE-Gd: MSN-Si-DMAE (0.401g); $GdCl_3.6H_2O$ (0.511 g); Yield: MSN-Si-DMAE-Gd (0.380 g). Elemental analysis (%) found: C 11.85, N 2.24, H 1.99, Gd 1.05.

MSN-Si-DMAE-Tb: MSN-Si-DMAE (0.407 g); $TbCl_3.6H_2O$ (0.526 g); MSN-Si-DMAE-Tb (0.420 g); Anal. Found (%) found: C 10.40, N 2.04, H 2.27, Tb 1.44.

MSN-Si-DMAE-Mn: MSN-Si-DMAE (0.401 g); $MnCl_2.4H_2O$ (0.281 g); MSN-Si-DMAE-Mn (0.440 g). Elemental analysis (%) found: C 11.41, N 2.22, H 2.46, Mn 1.07.

MSN-Si-DMAP-Gd: MSN-Si-DMAP (0.397 g); $GdCl_3.6H_2O$ (0.545 g); MSN-Si-DMAP-Gd (0.262 g). Elemental analysis (%) found: C 12.58, N 2.15, H 2.68, Gd 0.50.

MSN-Si-DMAP-Tb: MSN-Si-DMAP (0.362 g); $TbCl_3.6H_2O$ (0.536 g); MSN-Si-DMAP-Tb (0.305 g). Elemental analysis (%) found: C 11.45, N 2.00, H 2.68, Tb 0.38.

MSN-Si-DMAP-Mn: MSN-Si-DMAP (0.364 g); $MnCl_2.4H_2O$ (0.236 g); MSN-Si-DMAP-Mn (0.255 g). Elemental analysis (%) found: C 12.25, N 2.23, H 2.11, Mn 0.22.

3.4. Nanoparticle characterization

Proton Nuclear Magnetic Resonance spectra were performed using a Bruker AMX400 system (400,13 MHz). Data are indicated in the following order: solvent, chemical shift, spin multiplicity (s, singlet; t, triplet; m, multiplet), coupling constant (J in Hz), relative intensity (protons numbers). Fourier Transform infrared spectra were recorded on a Bruker tensor 27 system using the KBr pellet method under ambient conditions. The carbon, hydrogen, and nitrogen contents of the functionalized silica nanoparticles were obtained with a EuroVector EuroEA300 elemental analyser. Thermogravimetric analysis (TGA) was performed on a PerkinElmer STA6000 with a heating rate of 10 °C/min and under a 20 mL/min flow of He. Transmission electron microscopy (TEM) images were obtained using a Hitachi H-8100 microscope with thermionic emission (LaB6) and 200 kV acceleration voltage at MicroLAb (Instituto Superior Técnico). The average size of the nanoparticles was determined by manual counting using the Image J software. The samples were supported on carbon-coated copper grids and the digital image acquisition was performed with a CCD MegaView II bottom-mounted camera. Nitrogen adsorption-desorption isotherms at 77 K were determined on a Quantachrome Autosorb iQ system, using helium and nitrogen of 99.999% purity. Prior to the adsorption measurements, the samples were outgassed for 8 h at 180 °C (unmodified silica nanoparticles) or 80 °C (functionalized materials), with a heating rate of 1 °C/min. The X-ray diffraction (XRD) measurements were carried out on a Bruker AXS-D8 Advance powder diffractometer, using CuKα radiation (40 kV, 30 mA), with a step size of 0.01° (2θ) and 5 s per step. The particle size and zeta potential were measured using a Horiba SZ-100 system.

3.5. Cytotoxicity studies

The cell lines (3T3, 293T, HepG2, Caco-2) were previously acquired from DSMZ biobank. 3T3, Caco-2, HepG2 and 293T cells were cultured in Dulbecco´s Modified Eagle´s medium:

Nutrient Mix F-12 (DMEM/F-12) (Merck, Germany), in Minimum Essential Medium (MEM) (Merck, Germany), in RPMI medium (Sigma-Aldrich, USA), and in Dulbecco´s Modified Eagle´s medium (Merck, Germany), respectively, supplemented with 10% FBS (Hyclone, UK), 100 IU/mL penicillin, and 100 µg/mL streptomycin (Merck, Germany), and maintained in humidified atmosphere (95%), 5% CO_2 and 37 °C. Cytotoxicity of compounds (100 µg/ mL; 24 h) on cells viability was evaluated after they reached total confluence on 96-well plates. The effects were estimated by MTT assay (Sigma, Germany) and results expressed in percentage of control (%). Data are presented as mean ± standard error of the mean (SEM) and statistical analysis was performed using one-way analysis of variance (ANOVA) with Dunnett's multiple comparison of group means to determine significant differences relatively to control treatment. Differences were considered significant at a level of 0.05 (p - value < 0.05). Calculations were performed using GraphPad v5.1 (GraphPad Software, La Jolla, CA, USA) software.

4. Conclusions

Magnetic organic salts based on the combination of two choline derivatives cations [$N_{1,1,4,C2OH}$] and [$N_{1,1,4,C3OH}$] with anionic metal complexes [$MnCl_3$], [$GdCl_4$] and [$TbCl_4$] were synthesized. In order to reduce the eventual toxicity associated with the presence of metal complexes, their analogues were immobilized in MSNs. All materials were characterized by different techniques that confirmed the successful functionalization of MSNs with the cations [$N_{1,1,4,C2OH}$] and [$N_{1,1,4,C3OH}$]. Elemental analysis indicated 1.50 mmol/g of [$N_{1,1,4,C2OH}$] in MSN-Si-DMAE and 1.45 mmol/g of [$N_{1,1,4,C3OH}$] in MSN-Si-DMAP. For the final materials with the presence of $MnCl_3^-$, $GdCl_4^-$ and $TbCl_4^-$ as counter ions the ICP-MS results showed metal loadings in the range of 0.02-0.19 mmol/g with higher values for Si-DMAE cation, which can be related to possible steric effects resulting from the presence of a secondary alcohol in the Si-DMAP cation.

The cytotoxicity studies of the magnetic organic salts and their immobilized analogues were performed in four different cells 3T3, Caco-2, HepG2 and 293T. In general, the cytotoxic effects of the two cations are similar but there are relevant differences between the metal organic salts and their immobilized analogues. In the case of 3T3 cells, MSN-Si-DMAE-Mn exhibited a smaller cytotoxic effect than the corresponding metal organic salt. The system MSN-Si-DMAP-Gd presented a higher cytotoxic effect than [$N_{1,1,4,C3OH}$][$GdCl_4$] in the cases of 293T and Caco-2 cells and the same effect is observed for MSN-Si-DMAP-Tb in the case of 293T cells.

Some of these magnetic organic salts and nanomaterials can be interesting for further applications for biological detection or as contrast agents for magnetic resonance imaging (MRI). Higher chemical stability and biocompatibility using magnetic salts and silica nanoparticles can be achieved. Further studies such as NMR relaxation should be performed in order to evaluate their potential as MRI agents.

Conflicts of interest

There are no conflicts to declare.

Acknowledgements

This work was supported by National Funds through FCT/MCTES – Portuguese Foundation for Science and Technology within the scope of the projects UID/QUI/0619/2019, UIDB/50006/2020 (LAQV-REQUIMTE) and UIDB/00100/2020, UID/MAR/04292/2020 (MARE—Marine and Environmental Sciences Centre). Also, a doctoral fellowship to Andreia Forte (PD/BD/109625/2015) and Solchemar company are acknowledged. The NMR spectrometers are part of The National NMR Facility, supported by FCT/MCTES (RECI/BBB-BQB/0230/2012). Authors also thank to Prof. Madalena Dionísio and Dr. Natália Correia for support with the DSC analysis.

References

1 J. L. Vivero-Escoto, Ed., *Silica Nanoparticles, Preparation, Properties and Uses*, Nova Science Publishers, Inc., New York, USA, 2012.

2 A. Mehmood, H. Ghafar, S. Yaqoob, U. F. Gohar and B. Ahmad, *J. Dev. Drugs*, 2017, **6**, 1000174.

3 E. Yamamoto and K. Kuroda, *Bull. Chem. Soc. Jpn*, 2016, **89**, 501–539.

4 C. Bharti, U. Nagaich, A. K. Pal and N. Gulati, *Int. J. Pharm. Investig.*, 2015, **5**, 124–133.

5 S. Aparicio, M. Atilhan and F. Karadas, *Ind. Eng. Chem. Res.*, 2010, **49**, 9580–9595.

6 J. Kadokawa, Ed., *Ionic Liquids - New Aspects for the Future*, InTech, Rijeka, Croatia, 2013.

7 Z. Lei, B. Chen, Y. M. Koo and D. R. Macfarlane, *Chem. Rev.*, 2017, **117**, 6633–6635.

8 L. Nie, S. Yao, B. Dong, X. Li and H. Song, *J. Mol. Liq.*, 2017, **240**, 152–161.

9 S. Hayashi and H. Hamaguchi, *Chem. Lett.*, 2004, **33**, 1590–1591.

10 E. Santos, J. Albo and A. Irabien, *RSC Adv.*, 2014, **4**, 40008–40018.

11 G. Berselli, R. Vertechy and G. Vassura, *Smart Actuation and Sensing Systems - Recent Advances and Future Challenges*, InTech, Rijeka, Croatia, 2012.

12 A. Branco, L. C. Branco and F. Pina, *Chem. Commun.*, 2011, **47**, 2300–2302.

13 R. E. Del Sesto, T. M. McCleskey, A. K. Burrell, G. A. Baker, J. D. Thompson, B. L. Scott, J. S. Wilkes and P. Williams, *Chem. Commun.*, 2008, 447–449.

14 A. A. Rosatella, F. Siopa, R. F. M. Frade and C. A. M. Afonso, *New J. Chem.*, 2016, **40**, 3124–3129.

15 C. C. L. Pereira, S. Dias, I. Coutinho, J. P. Leal and L. C. Branco, *Inorg. Chem.*, 2013, **52**, 3755–3764.

16 R. F. M. Frade, S. Simeonov, A. A. Rosatella, F. Siopa and C. A. M. Afonso, *Chemosphere*, 2013, **92**, 100–105.

17 S. H. Zeisel and K. A. Da Costa, *Nutr. Rev.*, 2009, **67**, 615–623.

18 F. Siopa, T. Figueiredo, R. F. M. Frade, I. Neto, A. Meirinhos, C. P. Reis, R. G. Sobral, C. A. M. Afonso and P. Rijo, *Chemistry Select*, 2016, **1**, 5909–5916.
19 M. Bouchoucha, M. F. Côté, R. C-Gaudreault, M. A. Fortin and F. Kleitz, *Chem. Mater.*, 2016, **28**, 4243–4258.
20 C. I. C. Crucho, C. Baleizão and J. P. S. Farinha, *Anal. Chem.*, 2017, **89**, 681–687.
21 F. Rouquerol, J. Rouquerol and K. Sing, *Adsorption by Powders and Porous Solids*, Academic Press, London, United Kingdom, 1999.
22 M. Thommes, K. Kaneko, A. V. Neimark, J. P. Olivier, F. Rodriguez-Reinoso, J. Rouquerol and K. S. W. Sing, *Pure Appl. Chem.*, 2015, **87**, 1051–1069.
23 D. G. Capco and Y. Chen, Eds., *Nanomaterial, Impacts on Cell Biology and Medicine*, Springer Netherlands, Dordrecht, Netherlands, 2014.